Author(s): Sonnenschein, V.; Moore, Iain; Raeder, S.; Reponen, M.; Tomita, H.; Wendt, K.

Title: Characterization of a pulsed injection-locked Ti:sapphire laser and its application to high resolution resonance ionization spectroscopy of copper

Year: 2017

Version: Accepted version (Final draft)

Please cite the original version:

Sonnenschein, V., Moore, I., Raeder, S., Reponen, M., Tomita, H., & Wendt, K. (2017). Characterization of a pulsed injection-locked Ti:sapphire laser and its application to high resolution resonance ionization spectroscopy of copper. Laser Physics, 27(8), Article 085701. https://doi.org/10.1088/1555-6611/aa7834

Characterization of a pulsed injection-locked Ti:sapphire laser and its application to high resolution resonance ionization spectroscopy of copper

V Sonnenschein[1], I D Moore[3], S Raeder[4], M Reponen[2], H Tomita[1], K Wendt[4]

[1]Nagoya University, Furo-cho, Chikusa-ku, Nagoya, 464-8601, Japan
[2]RIKEN, 2-1 Hirosawa, Wako, Saitama 351-0198, Japan
[3]University of Jyväskylä - FI-40014, Jyväskylä, Finland
[4]Helmholtz Institute Mainz, Staudinger Weg 18, 55128 Mainz, Germany

E-mail: volker@nagoya-u.jp

Abstract. A high repetition rate pulsed Ti:sapphire laser injection-locked to a continuous wave seed source is presented. A spectral linewidth of 20 MHz at an average output power of 4 W is demonstrated. An enhanced tuning range from 710-920 nm with a single broadband mirror set is realized by the inclusion of a single thin birefringent quartz plate for suppression of unseeded emission. The spectral properties have been analyzed using both a scanning Fabry-Pérot interferometer as well as crossed beam resonance ionization spectroscopy of the hyperfine levels of natural copper. Delayed ionization of the long-lived excited state is demonstrated for increased resolution. For the excited state hyperfine coupling constant of the 244 nm $4s\,^2S_{1/2} \rightarrow 4s4p\,^4P^\circ_{1/2}$ ground-state transition in ^{63}Cu, a factor of ten reduction in error compared to previous literature was achieved. The described laser system has been in operation at several radioactive ion beam facilities.

Keywords: injection-locking, spectroscopy, hyperfine structure

PACS numbers: 32.10.Fn, 32.80.-t,42.55.-f,42.60.-v

Submitted to: *Laser Physics*

1. Introduction

At ISOL or IGISOL-type radioactive beam facilities [1, 2] laser resonance ionization offers outstanding opportunities to combine selectivity and sensitivity with an on-line ion source [3, 4]. The elemental selectivity of the technique, elucidated through the atomic level structure, has allowed for the production of purified radioactive beams, which are exploited in facilities dedicated to the study and applications of exotic nuclei. Inside the ion sources the atomic absorption line profiles are broadened by Doppler or pressure broadening effects. Typical pulsed laser systems aiming for the efficient and selective ionization of radioactive atoms possess spectral linewidths of several GHz, suitable for matching the broadened absorption profile.

Recently the implementation of resonance ionization spectroscopy (RIS) in a supersonic gas jet utilizing a narrowband first step excitation has initiated considerable interest [5]. Due to the cold environment created by the isentropic expansion of the gas, this novel in-gas jet spectroscopy technique can provide high-resolution data on isotope shifts and hyperfine structure in exotic atoms produced far from stability and in minute quantities. Such atomic studies yield direct information of nuclear properties such as spin, magnetic or electric moments and changes in charge radii between different isotopes [6]. This technique has been recently characterized in a measurement of actinium isotopes close to the $N = 126$ neutron shell closure [7]. Similar resolution, at least for heavy elements, may also be attained for hot-cavity ion sources when employing a crossed-beam geometry in the emitted atomic beam [8]. Duty-cycle losses can be partially compensated by shaping of the laser beams as well as the use of high laser pulse repetition rates. Laser spectroscopy may also be carried out after extraction from an ion source in a fast atom beam (after charge exchange) such as at the CRIS setup [9]. In addition to the extraction of nuclear information all these methods allows for the ionization of specific isotopes and isomers, or even the production of - at least to a significant extent - polarized ion beams by hyperfine level pumping. Corresponding developments are presently ongoing at a number of facilities worldwide to improve laser performance as well as experimental implementation.

To fully demonstrate and exploit the benefits of spectroscopy in these novel environments, a narrow linewidth ($< 100\,\mathrm{MHz}$), high power, pulsed laser source is desired. While a linewidth reduction of pulsed lasers is possible using additional intra-cavity wavelength filters [10, 11], this comes along with the disadvantage of reduced power levels. A better option is the pulsed amplification of a narrow-band continuous wave (cw) laser, either by dye or Titanium:sapphire (Ti:sapphire) amplifiers. As the emission cross section of dyes is up to three orders of magnitude higher, single- or few-pass amplification is sufficient there, though typical drawbacks accompanying dye lasers, such as safety hazards and higher maintenance requirements remain. For the lower gain Ti:sapphire crystal a repeated amplification is required to reach the desired final output power of several kW at the peak of the pulse from only few mW of cw input. This is best performed in a resonant cavity where the injected input beam (the

"seed") can be amplified and recycled over a large number of round-trips. For stable operation the cavity has to be kept in resonance with the frequency of the injected beam, requiring a stabilization or locking of the cavity length to a multiple of the seed wavelength. Drawbacks of this type of system are a higher complexity and less flexibility in wavelength range compared to the dye amplifier system, which can adapt the wavelength by choice of dye solution.

The purpose of this article is to provide a detailed technical description of the laser system to allow reproduction or modification by other interested groups as well as to document the improvements compared to previous prototypes. Secondly, by performing high resolution spectroscopy on a well-known hyperfine transition, a reference for the expected accuracy and resolution of the laser is provided. The developments and the spectroscopy discussed here have been carried out at the IGISOL facility in the Accelerator Laboratory of the University of Jyväskyä [14]. The system presented here has so far already been employed at the LISOL facility in Belgium [7, 12] and the CRIS laboratory at ISOLDE/CERN [13]. Furthermore off-line studies of several long-lived actinides (Th, Pu, Ac) have been performed in the LARISSA laboratory at the University of Mainz [14, 15]. While results from the cited applications already give an impression of the performance of the system, these primarily refer to the study of relatively unknown transitions in exotic isotopes. Furthermore, the introduction of a Ti:sapphire master laser as a seed source allowed for the first time a study of the laser performance over a wider range of wavelengths, as opposed to the relatively narrow isolated wavelength regions studied previously with diode laser sources.

The article is structured as follows: first the experimental setup of the injection-locked laser system is presented in section two, an evaluation of its performance is given in section three and section four details the application of this system to high resolution resonance ionization spectroscopy, concluding with a summary and outlook in section five.

2. Experimental setup

A layout of the injection-locked laser system is shown in figure 1. The figure highlights the continuous wave (cw) master laser, optical beam transport as well as the injection-locked Ti:sapphire cavity used for amplification and the electronics used for its stabilization. A prototype system similar to this was already described in [16]. Changes with respect to the earlier system can be found in the different seed source, changes to the locking setup and the introduction of a tunable quartz filter plate to extend the wavelength range. In the following the individual components are described.

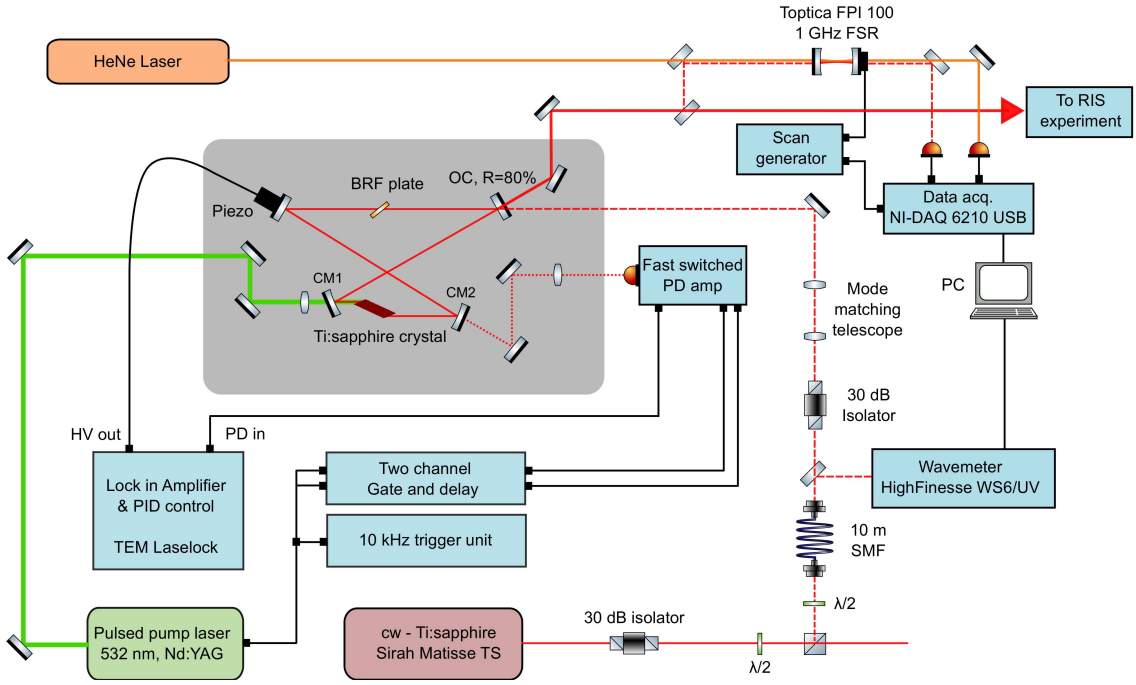

Figure 1: Overview of the injection-locked Ti:sapphire and the set-up used for injection-locking and spectral analysis.

2.1. Master laser

For stable operation of the system a master laser with a narrow short-term linewidth of less than 10 MHz is required. A power of a few mW is usually sufficient for generating the signal required for the locking electronics and to provide an efficient amplification resulting in an output signal with high spectral purity. In our case the input seed radiation to the injection-locked cavity is generated by a commercial cw Ti:sapphire laser (Sirah Matisse TS). With an input pump power of 6 W (Coherent, Verdi V6) and use of three different mirror sets the cw Ti:sapphire has an accessible wavelength range from 705-930 nm with a maximum output power of 1 W near 780 nm. For frequency stabilization the laser is locked to the side of a fringe of an external fiber-coupled high finesse reference cavity supplied by the manufacturer. The short-term frequency stability with respect to this reference cavity is typically less than 50 kHz when locked.

A small fraction of the cw output, about 10-100 mW, is separated from the main beam with a $\lambda/2$ plate and a polarizing beam-splitter (PBS) cube and coupled into a 10 m optical fiber for transport to the slave laser. 30 dB optical isolators before and after the fiber prevents feedback from the fiber tip and other surfaces to the cw Ti:sapphire in order to maintain stable single-mode operation as well as to prevent damage of the fiber from the high power pulses of the slave laser. Both standard single-mode (sm) and polarization maintaining (pm) fibers were tested, however even with the pm fiber system, noticeable short and long-term intensity fluctuations of the order of 10-20% remained, likely due to unstable environmental conditions. For optimal injection efficiency into the slave cavity, the mode profile of the fiber output is matched to that of the TEM_{00}

(fundamental Hermite-Gaussian) mode of the cavity using an adjustable telescope on a rail system.

2.2. Injection-locked slave cavity

The basic geometry of the injection-locked laser cavity was adapted from an initial design discussed in [16]. Compared to this prototype, which allowed flexibility for testing purposes, the new cavity uses mostly fixed geometry, simplifying the setup and alignment. The two curved mirrors CM1 and CM2 (radius of curvature = 75 mm) are aligned at a folding angle of $\alpha/2 = 17.75°$ for compensation of the Brewster-cut Ti:sapphire crystal-induced astigmatism. In the bow-tie shaped traveling wave resonator spatial hole burning effects are not present, making it much easier to attain stable single-mode operation. The dimensions of the cavity were set so that a single round-trip (0.5 m) in the bow-tie has about half the length of the Z-shaped cavities of the pulsed broadband Ti:sapphire lasers used regularly for resonance laser ionization at radioactive beam facilities [17, 18]. This should lead to comparable pulse durations and build-up times, as the gain medium is passed twice for a round-trip in the Z-shaped cavity, but only once in the bow-tie.

A lens with focal length $f = 75$ mm focuses the pump beam (Lee Laser LDP-200MQG, $M^2 \approx 20$) into the Ti:sapphire crystal. The crystal is wrapped in a thin layer of indium foil and enclosed within a two-part copper mounting structure. The bottom part of this mount is water-cooled, with the top part fixed on top of a peltier cooler for further reduction in temperature. The peltier (uwe electronic GmbH, UEPT-130-127-036E080E) is epoxy sealed to prevent damage from condensation and has a maximum power rating of 36 W. At low pump power levels condensation may occur on the crystal surface, which must be carefully prevented as it increases the risk of optically induced damage.

2.3. Cavity stabilization system

The baseplate of the laser cavity with dimensions of 45x25x1.5 cm^3 is made out of stainless steel and is supported by four posts using sorbothane damping feet (Thorlabs, AV2/M) to reduce high frequency vibrations, considering the cavity sits atop an undamped table. The feet have a resonance frequency of ≈ 15 Hz, so for this lower frequency range the isolation will be relatively poor. Higher frequency vibrations which may affect locking performance should however be reduced considerably. To stabilize the cavity to the seed laser the dither locking technique with phase sensitive detection is used [19]. To modulate and stabilize the cavity length one of the mirrors (Qioptiq Photonics GmbH, DLHS Ti:sapphire coating) with dimensions 12.7x5 mm is controlled by a piezo actuator (Piezomechanik GmbH, PSt 150-10-20 VS15) with a travel range of 27 μm and an unloaded resonance frequency of 30 kHz. The piezo actuator is connected to one of the two HV outputs of the servo drive or "lock-box" (TEM Messtechnik, Laselock 3.0 digital). This lock-box generates the error "lock-in" signal using the dithered piezo-

mirror. Furthermore it provides two independent PID regulators for feedback loops as well as different frequency filters to optimize the response of the system.

The input signal to the lock-box originates from the photodiode amplifier positioned behind mirror CM2. The leakage of the cw light through CM2 is used to stabilize the cavity to one of the transmission peaks. During and shortly after the pulse of the pump laser the incident light intensity on the detector will be orders of magnitude higher, leading to saturation of the photodiode and amplifier electronics. To allow for a quick recovery both are individually grounded during the pump pulse period using fast switches. The effect of this can be seen in the inset in figure 2, which shows the photodiode and error signal during a voltage ramp of the piezo. Using the 10 kHz trigger signal of the pump laser system as input, the timing signals for the switches are set up with a multi-channel gate and delay unit. Experimentally, a typical gate width of about 8 μs is used, several times longer than the fluorescence lifetime of the upper state laser level of the Ti:sapphire crystal (3.2 μs). As desired, the error signal is then only caused by the cw seed (see figure 2). Electrical noise due to the switches caused little detriment to the locking performance. A schematic of the switched amplifier circuit design developed at the University of Mainz can be found in [20, 21, 22] with a more recent version of the design available on request.

By monitoring the photodiode signal fluctuations at the flank of a transmission peak depending on the dither frequency, several strong mechanical resonances were observed in the frequency range from 10-30 kHz. To achieve a stable lock, the dither frequency was set to 42 kHz in a range with a relatively flat response, while the low-pass filter for the PID feedback was set to 2 kHz, far below the first observed resonance. When locked the photodiode voltage stays close to the transmission maximum, only with short interruptions by the switching (see figure 3).

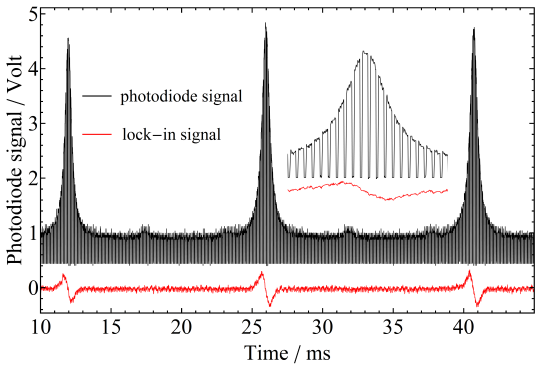

Figure 2: Photodiode and error signal during a piezo ramp. The inset shows the effect of the 10 kHz switching of the photodiode amplifier more clearly.

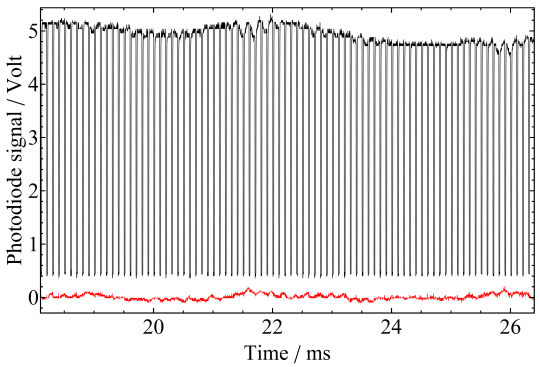

Figure 3: Photodiode and error signal during locking. The remaining signal fluctuations are mainly caused by intensity fluctuations of the cw input.

3. Results of the characterization of the resonator

3.1. Output power and linewidth measurements

With the laser locked to the seed laser at a wavelength of approximately 780 nm the output power and linewidth dependence on the pump power were investigated. The output power trend is displayed in figure 4, the three curves were measured after separate alignments of the cavity. At an output power of close to 5 W the damage threshold of the output coupling mirror was reached. With dedicated coatings for high average power, still higher output should be achievable. The slope of the efficiency curve above laser threshold was estimated to be about 0.45 and the optical-to-optical conversion efficiency from green to IR is about 30% for the maximum pump power. This efficiency is slightly higher compared to the conventional Z-shaped cavity Ti:sapphire lasers (20-25%), as is expected considering that no frequency selective elements such as a birefringent filter or etalon are needed for operation here.

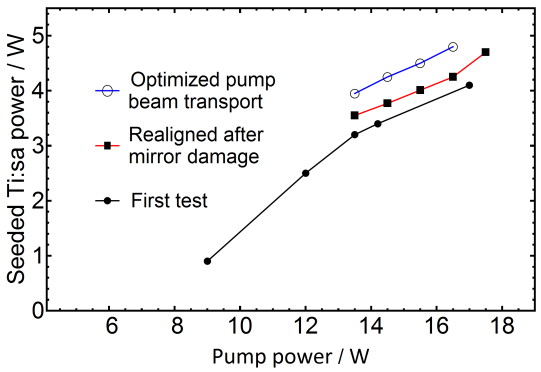

Figure 4: Output power vs. pump power for three alignment attempts of the cavity.

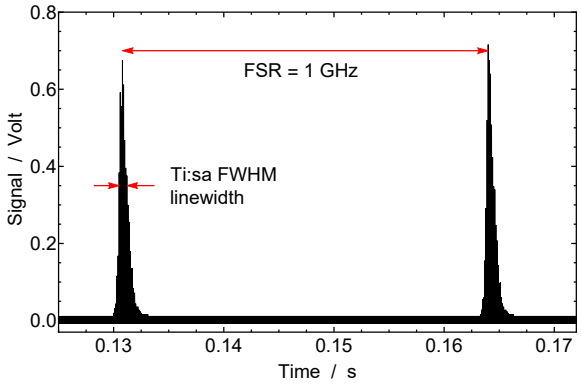

Figure 5: Linewidth measurement of the seeded laser output using a 1 GHz FSR FPI.

The spectrum of the injection-locked Ti:sapphire was measured using a commercial scanning Fabry-Pérot Interferometer (Toptica FPI-100-0750-1). It features a free spectral range (FSR) of 1 GHz and a Finesse F≈300 at 780 nm, measured using the continuous wave laser radiation of the cw master laser. As the injection-locked system is pulsed, the FPI spectra were taken with a slow scanning rate to allow for several individual pulses during a transmission peak of the FPI as shown in figure 5. Here two transmission peaks are visible, separated by the FSR of the FPI, and no side modes can be seen. The linewidth was measured for several pump power levels, which were estimated from a calibration curve. The dependence of the linewidth on pump power and output power is shown in Figs. 6 and 7, respectively. The minimum output linewidth may be estimated from the time-bandwidth product which should be 0.44 for a gaussian-shaped output pulse. While no pulse durations were measured at the time, close to the lasing threshold the typical pulse duration is > 100 ns, yielding a value of <4.4 MHz. Since the data indicates a linewidth of close to 10 MHz near the threshold, additional effects may influence the effective linewidth. As discussed in [23] the pump pulse can

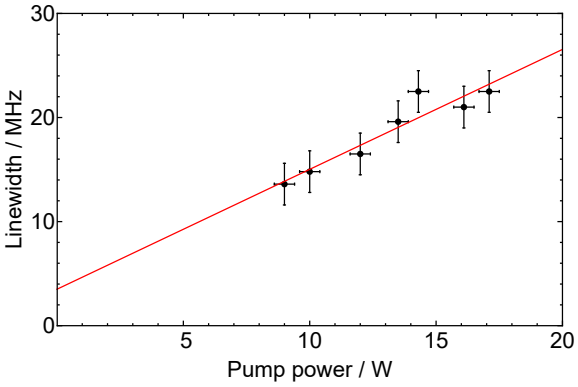

Figure 6: Linewidth of seeded Ti:sapphire laser versus pump power. Unvertainties in pump power are due to estimation from a calibration curve.

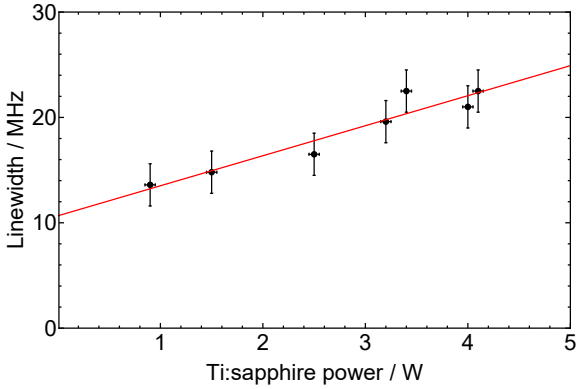

Figure 7: Linewidth of seeded Ti:sapphire laser versus output power

induce frequency chirp effects. Furthermore, the dithering of the cavity as well as locking stability could contribute to broadening. While not conclusive, chirp effects may indeed be one of the main factors contributing to the total linewidth. Accurate measurements of the pulse durations or alternatively the use of heterodyne techniques could further validate this assumption.

3.2. Wavelength tuning and birefringent filter plate

Changing the mirror set in order to reach certain wavelengths is inconvenient during experimental runs, where multiple transitions may be targeted within a short time span. While other modes have no starting boost provided by the injected laser, they may experience a much higher round-trip gain and thus outperform the mode at the seed wavelength. To estimate the limitations this puts on wavelength tunability a calculation was performed using multi-mode rate equations [24]. For these calculations the cavity mode at the seed wavelength was given a number of initial photons N_{seed} which was estimated from the injected power P_{inj} and the cavity round-trip time τ_{cav} as

$$N_{\mathrm{seed}} \approx \frac{P_{\mathrm{inj}}}{h \cdot \nu_{\mathrm{inj}}} \cdot \tau_{\mathrm{cav}}. \tag{1}$$

A more accurate estimate of this parameter would involve the power enhancement factor of the cavity as well as mode-matching inaccuracies. To reduce computational time not every possible individual mode was calculated, rather they were binned by wavelength into groups with similar gain. The results are displayed in figure 8, showing that for regions far off the gain peak of 800 nm unattainable amounts of input power would be required to reach a seed efficiency of 95%. The seed efficiency or spectral purity is the ratio of the power at the seed wavelength divided by the total output power. The expected tuning range of about 740-880 nm for a typical seed power of 10 mW is highlighted by the red vertical lines.

By suppression of the high gain region a wider tuning range should be possible. In low gain laser systems such as Ti:sapphire, birefringent filters are often used. As they are used for wavelength selection usually an expensive multi-plate filter is needed. This is not required in our case, since the final wavelength selection is determined by the cw seed. A simple single quartz plate is sufficient. To model the effect of the plate for proper choice of thickness the Jones matrix formalism [25] described in detail for birefringent filters in [26, 27] was applied. The round-trip matrix for the cavity is the product of the matrix for the quartz plate $M_{\mathrm{q}}(\theta, \phi, \lambda)$ as well as the polarization dependent gain/loss in the Ti:sapphire medium M_{t} and at the two Brewster surfaces M_{b} of the crystal, respectively. The round-trip intensity transmission coefficient can then be calculated from the eigenvalues (EV) as:

$$T = \mathrm{Max}\{\left|\mathrm{EV}[M_{\mathrm{q}}(\theta, \phi, \lambda) \times M_{\mathrm{b}} \times M_{\mathrm{t}} \times M_{\mathrm{b}}]\right|^2\}, \tag{2}$$

where the maximal values are chosen to represent the polarization eigenmode with the lowest loss. The angle θ is the angle between the surface normal and the incoming beam and is typically chosen as Brewster angle, while ϕ denotes the angle of rotation around the normal vector. The calculated dependence of T for a 235 μm thin quartz plate with the optical axis oriented perpendicular to the surface normal is shown in figure 9. The thickness was selected as a compromise between filtering resolution and the requirement of having no transmission maxima near the gain peak of the Ti:sapphire crystal. The filtering effect is strongest for an angle $\phi \approx 40°$ at which point transmission peaks are located at the far ends of the gain spectrum of the Ti:sapphire medium around 690 nm and 1020 nm. The quartz plate was supplied by Altechna with a specified accuracy of 235±10 μm.

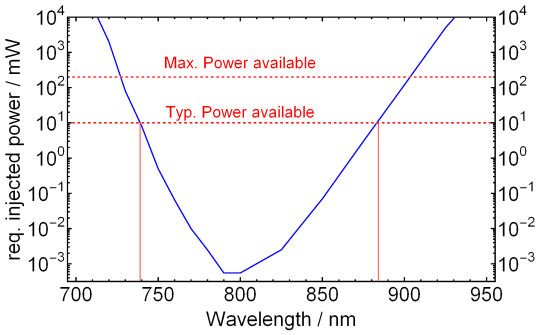

Figure 8: Simulation indicating the required seed power to reach 95% seed efficiency.

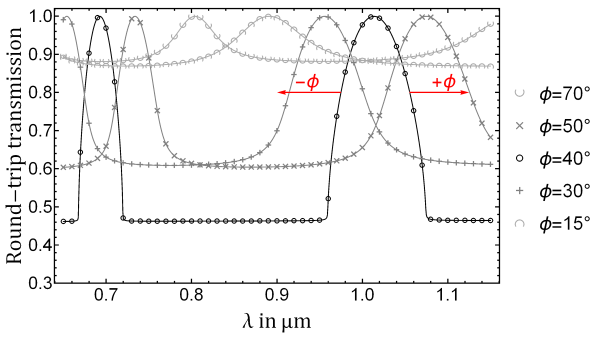

Figure 9: Angle tuning behaviour of the birefringent quartz plate.

The experimental tuning curve is illustrated in figure 10. In comparison, the rate equation calculations suggest a fairly similar tuning range for the case without the quartz plate. By inserting and properly adjusting the quartz plate, the tuning range could be extended from 735-880 nm to 715-920 nm. Experimentally the seed efficiencies are measured simply by comparing the uni-directional output power with and without seed. At maximum efficiency a factor of two increase in power is expected compared

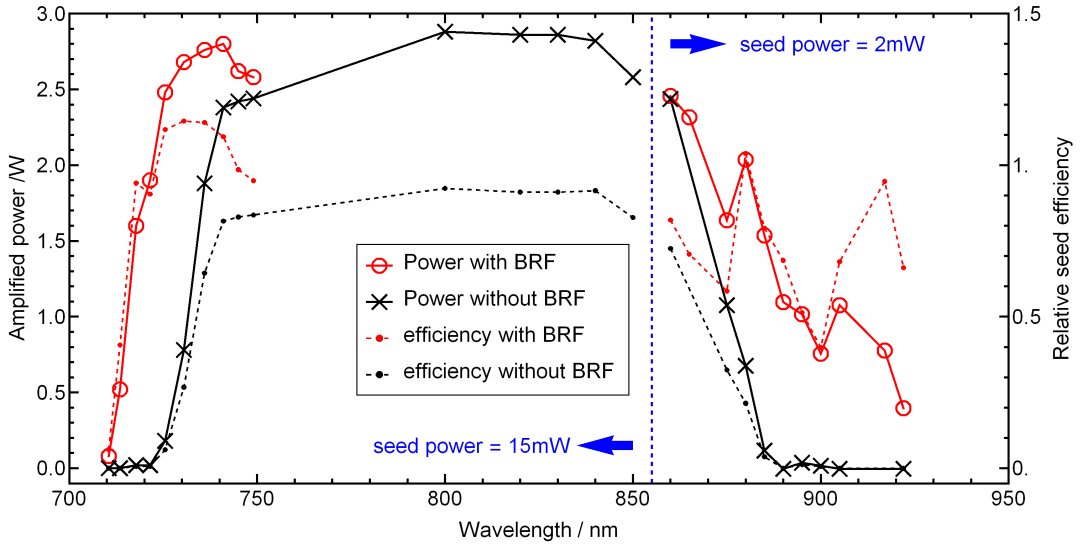

Figure 10: Wavelength tuning of the injection seeded laser with and without BRF plate.

to the free-running (bi-directional) output. In a few cases even stronger effects were seen, which may be due to lower losses of the resonator at the seed-wavelength or the reduced quantum defect at shorter output wavelengths. At the higher wavelength range fluctuations in the seed efficiency and output power are likely caused by losses on the mirror coatings. While the mirrors were coated for a wavelength range from 670-1050 nm, they were specified at 0° angle of incidence (AOI). At the 17.5° AOI used here, polarization dependence of the coating will start to impact the reflectivity, leading to higher than anticipated losses. A further limitation is the pump intensity used, which was lower compared to the typical values for Z-cavities (>20W). As the laser was operated at only a factor of two above lasing threshold during this measurement, the gain profile of the Ti:sapphire medium sets obvious limits. Due to the double-pass through the crystal in Z-cavities the typically chosen output coupler reflectivity of 70-80% would equate to a value of R=85-90% in the bow-tie resonator. An increase to these more comparable values will widen the tuning range further. Additionally it has been shown that positioning the gain medium closer to the resonator focus improves the roundtrip-gain, though at the cost of total output power.

4. Hyperfine spectroscopy in stable copper isotopes

To test the suitability of the injection-locked Ti:sapphire laser for high-resolution spectroscopy in combination with a precise relative wavelength monitoring system, the hyperfine structure (hfs) of stable copper isotopes was measured using a two-step RIS scheme in a small compact atomic beam unit (ABU). The RIS scheme requires a wavelength of 244.237 nm for the first excitation step from the atomic ground state - $3d^{10}4s\ ^2S_{1/2}$ - to the excited state at 40943.73 cm^{-1} - $3d^9(^2D)4s4p(^3P^\circ)^4P^\circ_{1/2}$ - and 441.679 nm for the second step to an autoionizing state at 63584.57 cm^{-1} as discussed

in [11].

4.1. Experimental details

By employing the quartz plate in the injection-locked Ti:sapphire an output power of 2.8 W at a wavelength of 732.71 nm was produced using a pump power of about 12 W. The first step wavelength was then generated by third harmonic generation, with up to 50 mW of UV light available, reduced to 30 mW after transport losses. The spot of the UV beam at the atomic beam - laser interaction region was slightly elliptical with dimensions of 2x5 mm^2 estimated by eye. This equates to an intensity of 300 mW/cm^2 or 30 $\mu J/cm^2$ at 10 kHz. The UV power can easily be adjusted by rotating the polarization state of one of the input beams to the frequency-tripling crystal. For the second step excitation an intra-cavity frequency-doubled broadband Ti:sapphire [28, 29] was employed with 0.8 W power at the interaction region. The spot size of the blue laser was $\approx 0.5\,cm^2$, yielding 1.6 W/cm^2. In this setup, the two Ti:sapphire systems were pumped using two separate Nd:YAG lasers. While this results in a slightly larger timing jitter of about 10 ns, it also allows for an easy synchronization or controlled delay time ΔT as shown in figure 11.

Wavelength changes of the cw seed were measured using the Toptica scanning FPI by comparing its transmission fringe positions to those of a stabilized HeNe laser. By scanning the piezo actuator over several free spectral ranges its movement could be approximated by a third order polynomial, which allows for accurate compensation of nonlinearities. The FSR of 0.998604(14)$\dot{\text{G}}$Hz of the FPI was calibrated using saturated absorption spectroscopy of Rubidium [30, 14].

The atomic beam is created by resistively heating a copper sample inside of a tantalum tube and is collimated at a distance of 5 cm with a 0.5 mm slit. A repelling voltage of typically 70 V is applied to the slit in order to suppress surface ions, as seen in figure 12. The atoms are resonantly ionized and focused onto an electron multiplier tube (EMT). The current from the EMT is then amplified using a picoamperemeter and its output voltage is monitored using a NI-DAQ 6210 data acquisition system.

4.2. Analysis and results

Several scans at different UV power levels and for different delay times of the ionization step were acquired. The scan at full power (30 mW) and zero delay is shown in figure 13. Errors of data-points were estimated from the standard-deviation of the signal within a binning interval of 15 MHz. Each hyperfine component of the stable ^{63,65}Cu isotopes except for a slight overlap of the last pair at the higher frequency end are well separated. To fit the data a multi-peak Voigt profile is used:

$$\mathrm{Y}(\nu) = S \cdot \sum_{i=1}^{N} \psi_i y_i \mathrm{Voigt}[w_\mathrm{G},\, w_\mathrm{L} \cdot \gamma_i,\, \nu - \nu_\mathrm{cog} - \nu_i(A,B) - \Delta]. \qquad (3)$$

The equation is given for one isotope only, with overall signal amplitude S and Gaussian and Lorentzian widths w_G and w_L, respectively. The hyperfine coupling constants A

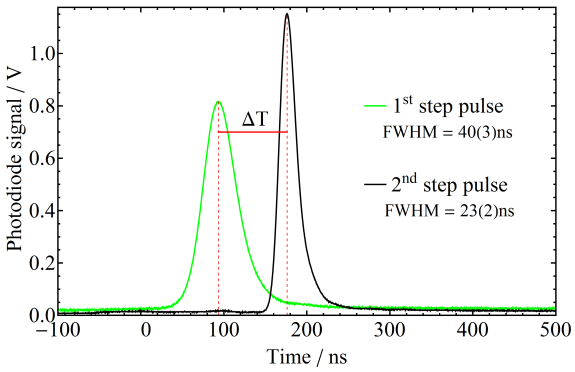

Figure 11: Pulse durations and delay between the excitation lasers monitored by fast photodiodes.

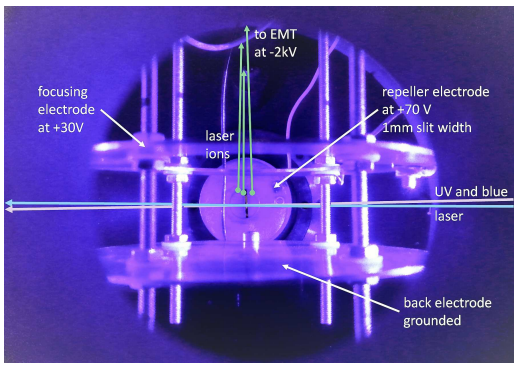

Figure 12: View looking into the atomic beam unit (ABU) showing the collimating slit and ion optics. The atomic beam is perpendicular to the page.

and B, which determine the resonance frequencies ν_i of the hyperfine components are fitted. The signal strength for the individual hyperfine components are the y_i values calculated using the 6j-Symbols [31]. Further fit parameters are the center of gravity ν_{cog} of a chosen reference isotope, the isotope shift Δ with respect to this isotope as well as ψ_i and γ_i, which represent modifications to the individual intensities and Lorentzian linewidths for each hyperfine component, which can occur due to optical pumping and saturation effects. The signal ratio between the isotopes was not fixed to the natural abundance ratio ^{63,65}Cu (0.6915 : 0.3085), but kept free to better accommodate slight intensity fluctuations of the lasers.

The Voigt profile was implemented in Mathematica (code available on request) using a fast numerical approximation based on a Fourier expansion as discussed in [32]. To demonstrate the effect of additional parameters on the quality of fit, residuals are plotted in the lower panel of figure 13 for four individual fits of the same dataset along with reduced chi-square values. Fit A uses line intensities fixed to the theoretically calculated ones, while Fit B allows for changes of intensity (parameter ψ_i). Free Lorentzian linewidths (parameter γ_i) are additionally included in Fit C, and Fit D further allows for a mix of two ensembles of atoms with different Lorentzian widths. Since the laser beams have an approximately Gaussian intensity profile, atoms in the center of the beams will experience stronger saturation effects than those located at the tails of the intensity profile. This is qualitatively accounted for in Fit D, which shows a noticeable improvement on the residuals. At lower saturation levels however the effect is less pronounced and fit parameters showed strong dependence on initial values. Due to this, Fit C was used for better inter-comparability in the following.

The averaged results for the hyperfine parameters and the isotope shift, including comparisons with our previous (lower resolution) experiment [11] and literature data, are shown in Table 1. The errors given in round brackets include only the error estimated from the statistical variation between the scans, while the error value in square brackets

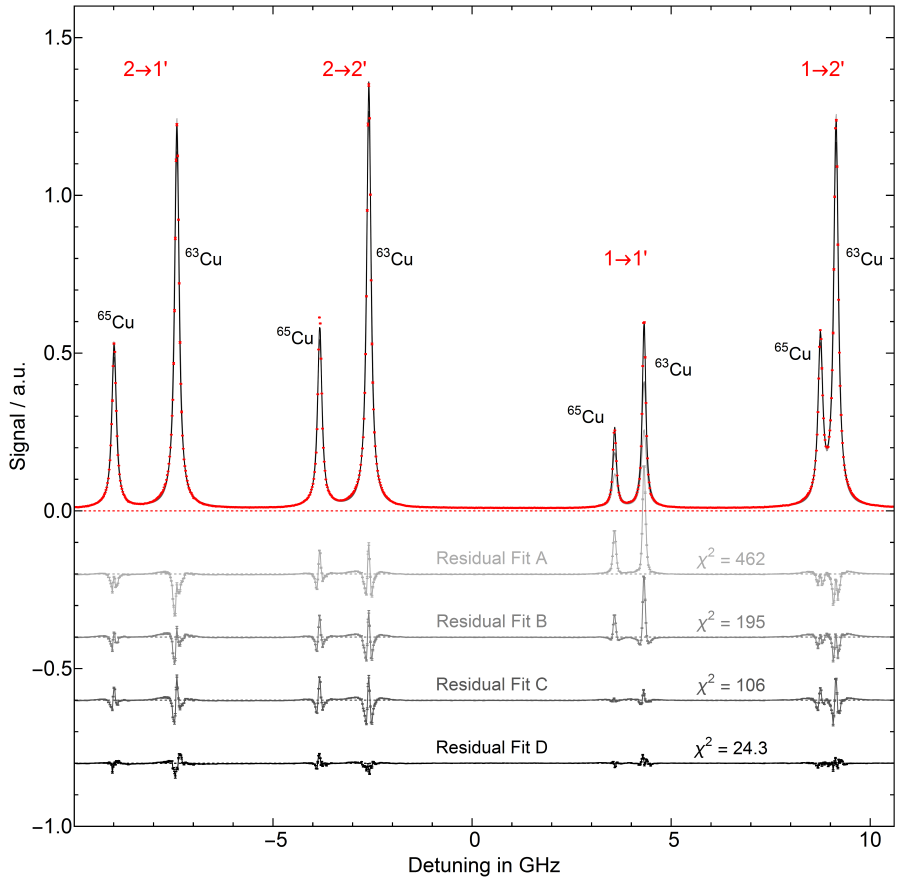

Figure 13: Single scan of the 244 nm transition in Cu I illustrating the hyperfine structure. Data points in red, fitted Voigt curve in black. The components are marked by their respective isotope and individual F→F' transition. The lower panel shows the fit residuals for the different fits A-D, slightly offset for clarity.

includes the uncertainty of the FSR and remaining non-linearity of the FPI calibration of the fringe positions not accounted for by the simple polynomial model. While the ground state splitting (A_g) in Cu is known with very high precision [33], the excited state (A_e) values have previously only been measured with lower resolution using pulsed lasers [34]. In the excited state of ^{63}Cu the literature value is less precise and does not agree within 2.5 σ. The same is true for the isotope shift value with a deviation of more than 3 σ. It is likely that the errors for the literature values from [34] were underestimated, considering that a much wider spectral width of > 3 GHz and less accurate wavelength determination was used in their work. In [34] a ratio for the excited (e) and ground state (g) hyperfine parameters was extracted with values of A_e/A_g=0.415(2) for ^{63}Cu and 0.412(3) for ^{65}Cu. Our experimental values are A_e/A_g=0.41101(30) for ^{63}Cu and 0.41095(30) for ^{65}Cu, showing a smaller variation between the isotopes.

The optimal spectral resolution in this experiment was 47(4) MHz FWHM for the Gaussian - and 16(6) MHz for the Lorentzian contribution to the Voigt profile. The Gaussian contribution Δw_G is caused in approximately equal parts by the

Table 1: Experimental results for hyperfine coupling constants of ^{63}Cu and ^{65}Cu and their isotope shift. Comparison with literature values from [34](†) [33](*) and our previous result using the dual-etalon version of the Ti:sapphire laser [11] are given. For the dual-etalon measurement no result is given for ^{65}Cu as a fixed ratio A^{63}/A^{65}=5.867/6.284 was used for the fit.

Parameter	This exp.	Literature	prev. exp.[11]
^{63}Cu A_g/MHz	5867.06(15)[116]	5866.908706(20)*	5887(20)
^{63}Cu A_e/MHz	2411.25(25)[86]	2432(8)†	2416(20)
^{65}Cu A_g/MHz	6284.82(20)[121]	6284.389972(60)*	-
^{65}Cu A_e/MHz	2582.33(18)[87]	2588(15)†	-
ΔIS^{63-65}Cu /MHz	1046.41(33)[79]	977(21)†	1090(100)

laser linewidth Δw_l of about 34(5) MHz (increased by a factor $\sqrt{3}$ due to the third harmonic) and Doppler broadening Δw_D, which can be calculated either from $\Delta w_D = \sqrt{(\Delta w_G)^2 - (\Delta w_l)^2} = 30(6)$ MHz or from the collimating angle α and the Maxwell-Boltzmann distribution as $\Delta w_D = \alpha/\lambda \cdot \sqrt{8 k_b T \ln(2)/m_{\mathrm{Cu}}} = 27(4)$ MHz for α =10(1) mrad and T=1100(100) K.

4.3. Saturation and delay effects

Two series of measurements, with a combined total of 12 scans of the hyperfine structure were performed. In the first series, the delay time between the laser pulses was kept fixed at $\Delta T \approx 0(5)$ ns, while the power of the first excitation step was varied. For the second series, the first excitation step was kept at maximum intensity, while the ionization step was delayed. The effect of saturation on the ion signal rate S is shown in figure 14. The data is fitted using a standard two-level atom saturation curve

$$S(I) = S_0 \cdot \frac{I/I_{\mathrm{sat}}}{1 + I/I_{\mathrm{sat}}}, \tag{4}$$

resulting in a saturation intensity I_{sat} of 30.6(14) mW/cm^2. The Lorentzian component of the Voigt profile w_L also shows a saturating behavior as illustrated in figure 15, along with two different fit models. One model (blue dashed line) follows the expected behavior of a two-level atom with $w_L(I) \propto \sqrt{1 + I/I_{\mathrm{sat}}}$ yielding I_{sat}=44(5) mW at a reduced chi-square of $\chi^2_r = 2.9$. The other model (red line) includes an additional offset term, representing other factors causing a Lorentzian-shaped line broadening, yielding I_{sat}=7(5) mW ($\chi^2_r = 1.5$). The disagreement between the three extracted saturation intensities - and the fact that the Lorentzian linewidth is much larger than expected from the natural linewidth of the transition - indicates that the model is insufficient and additional factors need to be considered.

One such factor is the ionization laser, influencing the excited state through the AC stark effect caused by its high intensity as well as by the coupling to the autoionizing state. A model describing these additional effects, applied to this dataset, has been published separately [35]. This model suggests that by delaying the ionization laser

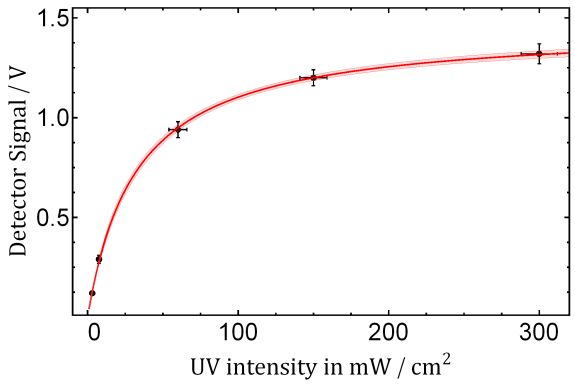

Figure 14: Ion signal versus incident first step laser intensity.

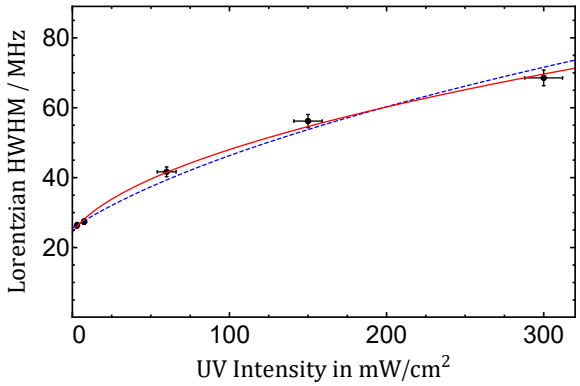

Figure 15: Lorentzian HWHM parameter versus first step laser intensity.

with respect to the probe laser used for spectroscopy the spectral broadening effects can be minimized with negligible loss in efficiency for a long-lived excited state.

In the ionization scheme of Cu two known decay channels of the first excited state exist [36]. One to the ground state ($\Gamma_1 = 2.03 \cdot 10^6\,\mathrm{s}^{-1}$) and another one to a level at $13245.423\,\mathrm{cm}^{-1}$ ($\Gamma_2 = 3.99 \cdot 10^4\,\mathrm{s}^{-1}$), resulting in a lifetime of the state of $\tau = 1/\sum\Gamma_i = 483\,\mathrm{ns}$. This is much longer than the duration of the laser pulses with $40(3)\,\mathrm{ns}$ and $23(2)\,\mathrm{ns}$ for the first and second step laser, respectively. The pulse durations are given for the fundamental laser radiation for the first step laser and for the second harmonic for the second step. The delay between the two laser pulses was varied between 0-600 ns. Figure 16 shows the ion signal amplitude dependence and figure 17 the linewidth dependence. The benefit of the delay is immediately obvious. While the linewidth drops noticeably even for a short delay of 40 ns, the ion signal is only impacted very slightly due to the slow decay of the excited state population. The lifetime of the excited state was extracted by a fit using either all data points as $\tau = 472(43)\,\mathrm{ns}$, or only the last four data points, which exhibit minimal influence from the ionization laser as $\tau = 462(71)\,\mathrm{ns}$. While these values agree quite well with the literature data, the method used here is sensitive to several parameters, in particular the beam-spot shape and the spatial overlap of the laser spots. Since the atoms move slightly in the delay time between the laser pulses, misalignments and the intensity distributions of the lasers could affect the results.

5. Conclusion and outlook

An injection-locked Ti:sapphire laser has been developed and its performance has been characterized. A wide tuning range with a single mirror set was made possible by a simple single-plate quartz filter, allowing for flexible choice of atomic transitions. While the first time setup of the system requires some time investment (1-3 days by experienced personnel), after installation only little additional interaction is needed to maintain operational conditions compared to the standard Z-cavity lasers. The relative ease of

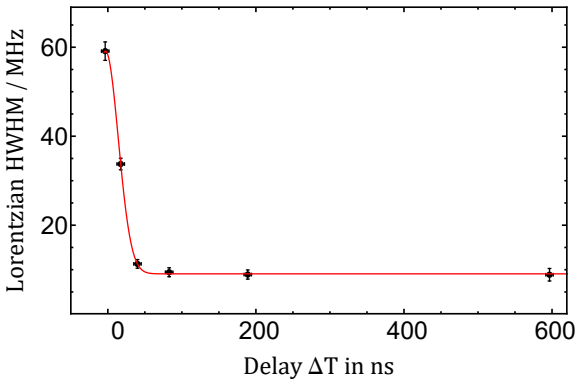

Figure 16: Lorentzian HWHM parameter versus delay of ionization laser. Data points in black, Gaussian fit in red.

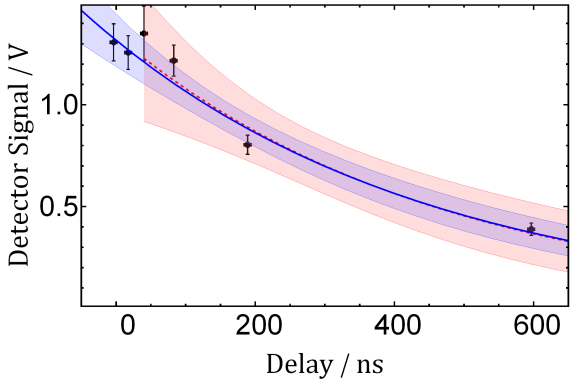

Figure 17: Ion signal versus delay of ionization laser. Data points in black, fits and 90% confidence intervals in red, dashed (four points) and blue (all points).

use, transportability and reliability of the system has been proven by its utilization at several facilities with varying users of the experimental setup. The spectral width of $<$20 MHz of the system, which is of the same order as the natural linewidth of many strong atomic transitions makes it an ideal choice for any RIS experiment which is not limited by pressure or Doppler broadening effects.

Currently an updated design of the cavity is under review. It will provide higher passive stability against vibrations optimized using finite element analysis (FEA), as well as the inclusion of fiber coupling and mode-matching optics on the laser baseplate. This will further aid in transport and ease of setup of the system. A further extension of the tuning range by improvement of the pump beam geometry is under study.

In the application of the laser system to high resolution spectroscopy in copper a direct comparison with high precision literature values showed excellent agreement within the error margin. The wavelength calibration and control of the seed laser is likely the main factor limiting the precision of the measurements and is critical to any similar experiment. Nevertheless, the MHz-level uncertainty is sufficient for most of the envisaged applications of the system, e.g. for spectroscopy on heavy elements, as discussed for instance in [7]. The possible incorporation of delayed ionization with only minor losses in signal will further fortify these studies, and bring the in-gas jet and cross-beam resonance ionization techniques to full fruition.

Acknowledgments

This work was supported by the Academy of Finland under the Finnish Centre of Excellence Programme 2012-2017 (Project No. 213513, Nuclear and Accelerator-Based Physics Research at JYFL). This project has also received funding from the European Unions Horizon 2020 research and innovation programme under grant agreement No 654002 (ENSAR2).

References

[1] Blumenfeld Y, Nilsson T and Duppen P V 2013 *Phys. Scripta* **2013** 014023 URL http://stacks.iop.org/1402-4896/2013/i=T152/a=014023

[2] Äystö J *et al.* 2014 *IGISOL: Three decades of research using IGISOL technique at the University of Jyväskylä* SpringerLink : Bücher (Springer Netherlands) ISBN 9789400755550 URL https://books.google.co.jp/books?id=4gTGBAAAQBAJ

[3] Marsh B A 2014 *Review of Scientific Instruments* **85** URL http://scitation.aip.org/content/aip/journal/rsi/85/2/10.1063/1.4858015

[4] Fedosseev V N, Kudryavtsev Y and Mishin V I 2012 *Phys. Scripta* **85** 058104 URL http://stacks.iop.org/1402-4896/85/i=5/a=058104

[5] Kudryavtsev Y *et al.* 2013 *Nucl. Instrum. Meth. Phys. Res. B* **297** 7 – 22 ISSN 0168-583X URL http://www.sciencedirect.com/science/article/pii/S0168583X12007525

[6] Campbell P, Moore I D and Pearson M R 2016 *Prog. Part. Nucl. Phys.* **86** 127 – 180 ISSN 0146-6410 URL http://www.sciencedirect.com/science/article/pii/S0146641015000915

[7] Ferrer R *et al.* 2017 *Nat. Comm.* **8** URL http://dx.doi.org/10.1038/ncomms14520

[8] Heinke R *et al.* 2016 *Hyperfine Interact.* **238** 6 ISSN 1572-9540 URL http://dx.doi.org/10.1007/s10751-016-1386-2

[9] Cocolios T *et al.* 2013 *Nucl. Instr. Meth. Phys. Res. B* **317, Part B** 565 – 569 ISSN 0168-583X {XVIth} International Conference on ElectroMagnetic Isotope Separators and Techniques Related to their Applications, December 27, 2012 at Matsue, Japan URL http://www.sciencedirect.com/science/article/pii/S0168583X13007088

[10] de Groote R *et al.* 2015 *Phys. Rev. A* **92**(2) 022506 URL http://link.aps.org/doi/10.1103/PhysRevA.92.022506

[11] Sonnenschein V *et al.* 2014 *Hyperfine Interact.* **227** 113–123 ISSN 0304-3843 URL http://dx.doi.org/10.1007/s10751-013-1000-9

[12] Raeder S *et al.* 2016 *Nucl. Instrum. Meth. Phys. Res. B* **376** 382 – 387 ISSN 0168-583X Proceedings of the XVIIth International Conference on Electromagnetic Isotope Separators and Related Topics (EMIS2015), Grand Rapids, MI, U.S.A., 11-15 May 2015 URL http://www.sciencedirect.com/science/article/pii/S0168583X15012586

[13] de Groote R P, Lynch K M and Wilkins S G 2016 *Hyperfine Interact.* **238** 5 ISSN 1572-9540 URL http://dx.doi.org/10.1007/s10751-016-1378-2

[14] Sonnenschein V 2015 *Laser Developments and High Resolution Resonance Ionization Spectroscopy of Actinide Elements* Ph.D. thesis University of Jyväskylä

[15] Voss A *et al.* 2017 *Phys. Rev. A* **95**(3) 032506 URL https://link.aps.org/doi/10.1103/PhysRevA.95.032506

[16] Kessler T *et al.* 2008 *Laser Phys.* **18** 842–849 ISSN 1054-660X URL http://dx.doi.org/10.1134/S1054660X08070074

[17] Mattolat C *et al.* 2009 *AIP Conference Proceedings* **1104** 114–119 URL http://aip.scitation.org/doi/abs/10.1063/1.3115586

[18] Rothe S *et al.* 2011 *Journal of Physics: Conference Series* **312** 052020 URL http://stacks.iop.org/1742-6596/312/i=5/a=052020

[19] White A D 1965 *Quantum Electronics, IEEE Journal of* **1** 349–357 ISSN 0018-9197

[20] Tomita H *et al.* 2008 *J. Nucl. Sci. Technol.* **45** 37–42 URL http://dx.doi.org/10.1080/00223131.2008.10875974

[21] C Mattolat 2010 *Spektroskopische Untersuchungen an Technetium und Silizium - Ein Festkörperlasersystem für die Resonanzionisationsspektroskopie* Ph.D. thesis University of Mainz

[22] Kessler T 2008 *Development and application of laser technologies at radioactive ion beam facilities* Ph.D. thesis University of Jyväskylä

[23] Hannemann S, van Duijn E J and Ubachs W 2007 *Rev. Sci. Instrum.* **78** 103102 URL http://scitation.aip.org/content/aip/journal/rsi/78/10/10.1063/1.2789690

[24] R E Horn 2003 *Aufbau eines Systems gepulster, abstimmbarer Festkörperlaser zum Einsatz in der Resonanzionisations-Massenspektrometrie* Ph.D. thesis University of Mainz
[25] Jones R C 1941 *J. Opt. Soc. Am.* **31** 488–493
[26] Yang T, Jing H and Liu D 2006 *J. Opt. A* **8** 295 URL http://stacks.iop.org/1464-4258/8/i=3/a=011
[27] Yang T *et al.* 2007 *J. Opt. A* **9** 222 URL http://stacks.iop.org/1464-4258/9/i=3/a=002
[28] Reponen M *et al.* 2012 *Eur. Phys. J. A* **48** 45 ISSN 1434-601X URL http://dx.doi.org/10.1140/epja/i2012-12045-2
[29] Sonnenschein V *et al.* 2015 *JPS Conf. Proc.* **6** 030126 URL http://journals.jps.jp/doi/abs/10.7566/JPSCP.6.030126
[30] Geldhof S *et al.* 2016 *Hyperfine Interact.* **238** 7 ISSN 1572-9540 URL http://dx.doi.org/10.1007/s10751-016-1385-3
[31] Drake G W F 2006 *Springer Handbook of Atomic, Molecular, and Optical Physics* Springer Handbook of Atomic, Molecular, and Optical Physics (Springer) ISBN 9780387263083 URL http://books.google.de/books?id=Jj-ad_2aNOAC
[32] Abrarov S M and Quine B M 2011 *Appl. Math. Comput.* **218** 1894 – 1902 ISSN 0096-3003 URL http://www.sciencedirect.com/science/article/pii/S0096300311009179
[33] Figger H, Schmitt D and Penselin S 1967 *Colloq. Int. C.N.R.S* **164** 355
[34] Cocolios T E *et al.* 2010 *Phys. Rev. C* **81**(1) 014314 URL http://link.aps.org/doi/10.1103/PhysRevC.81.014314
[35] de Groote R *et al.* 2017 *Phys. Rev. A* **95**(3) 032502 URL http://link.aps.org/doi/10.1103/PhysRevA.95.032502
[36] RL Kurucz and B Bell 1995 *Smithsonian Astrophysical Observatory.* URL http://www.pmp.uni-hannover.de/cgi-bin/ssi/test/kurucz/sekur.html